This article has been accepted for publication in a future issue of this journal, but has not been fully edited. Content may change prior to final publication. Citation information: DOI 10.1109/TDEI.2022.3173497, IEEE Transactions on Dielectrics and Electrical Insulation

Modelling of Internal Pressure Dynamics in Mass-Impregnated Non-Draining HVDC Cables

Ø. Hestad, M. Runde, H. Enoksen and **N. Magnusson**
SINTEF Energy Research,
NO-7465 Trondheim, Norway

ABSTRACT

Changing the current loading of mass-impregnated non-draining power cables causes the pressure in the insulation to vary over a wide range. It is generally recognized that under certain conditions—typically after a large load reduction—the pressure becomes so low that shrinkage cavities (voids) form in the insulation, and that partial discharges that may damage the insulation ignite. A finite element model for temperature, electric field and pressure dynamics throughout the insulation layer has been developed. Comparisons with previously obtained measurements on full-scale HVDC subsea cable samples subjected to a variety of loading patterns, external pressures (sea depths) and ambient temperatures, show that the model replicates the pressure behavior of the insulation reasonably well. Most importantly, the complicated viscoelastic properties of the lead sheath, which have a profound effect on the internal pressure dynamics and thereby on the prospects of forming potentially harmful cavities, appear to be sufficiently accurately modelled.

Index Terms — HVDC insulation, power cables, impregnated insulation, numerical modelling

1 INTRODUCTION

MASS-IMPREGNATED non-draining (MIND) cables have been the technology of choice for HVDC interconnections involving long sea crossings, e.g., in the North Sea and the Mediterranean. The electrical insulation system of such cables consists of around 200 layers of 2–3 cm wide lapped paper or polypropylene laminated paper tapes impregnated with a high-viscosity oil, often referred to as the "mass" [1]. The most recent projects typically include cables operating at 500 kV / 1400 A with an approximately 20 mm thick insulation.

A characteristic feature of the insulation is that the thermal expansion and contraction of the two materials involved differ greatly. The volumetric thermal expansion coefficient of the mass is ten times that of the paper [2]. This affects how the insulation behaves when the current loading changes and the cable heats up or cools down. It has for long been generally accepted that under certain conditions shrinkage cavities or voids form in the insulation [2–5]. A load turn-off is the prime example of such a condition.

The dielectric strength of the cavities is lower than in the surrounding impregnated insulation, so when exposed to high electrical fields partial discharges (PDs) may occur in these cavities. It is also generally recognized that the PDs may or may not be powerful enough to cause local and permanent damage to the insulation. Extensive PD-induced carbonization may develop into a complete breakdown. The dielectric type test applied for MIND cables [6] includes extensive load cycling duties to confirm that a cable can handle the potential problems associated with shrinkage cavities.

During the cable manufacturing process both paper and mass are carefully treated to remove humidity and gaseous components [5]. Consequently, cavities will only be created when the internal pressure in the insulation is low, ostensibly well below atmospheric. The prospects of having cavities formed are thus clearly related to the internal pressure in the insulation, which for a given cable is determined by a multitude of design, operational and environmental factors.

Recently, the pressure in the insulation of 4–5 m long MIND cable samples subjected to current cycling, different ambient temperatures and pressures has been recorded in laboratory experiments [7–9]. Internal pressures ranging from 0 to more than 30 bar were measured in a cable kept in a normal indoor ambient. Moreover, pressure measurements at the innermost and outermost parts of the insulation revealed that under fast and large load changes a considerable radial pressure gradient appears in the insulation. If maintained for some time, this gradient produces a radially directed migration of mass through the paper layers, leading to a redistribution of the mass in the insulation. It was also demonstrated how an external pressure—typically the surrounding water pressure of a subsea installation—influences on the radial pressure dynamics and

Manuscript received on 16 August 2021, in final form 25 April 2022, accepted 25 April 2022. Corresponding author: M. Runde.

This article has been accepted for publication in a future issue of this journal, but has not been fully edited. Content may change prior to final publication. Citation information: DOI 10.1109/TDEI.2022.3173497, IEEE Transactions on Dielectrics and Electrical Insulation

distribution in the insulation. Furthermore, slow mechanical deformations in the lead and polyethylene (PE) sheaths were found to also have a significant impact on the internal pressure behavior.

Consequently, predicting under what conditions the pressure in MIND cable insulation drops to levels where cavities may form becomes complicated, as it involves a host of material, operational and environmental parameters. The only conceivable method is to develop a numerical model and verify it by comparing the output with measurements obtained on full-scale cables. This is the approach taken in the work presented here. The model also calculates electric field and temperature distributions, a much simpler task when the mass-impregnated paper is assumed to be a homogeneous medium, i.e., disregarding effects of its layered structure and the butt gaps.

Work on modelling the internal pressure dynamics of MIND cables found in the open literature is scarce, despite the profound effect low pressures and shrinkage voids may have on this insulation system. Szabo et al. developed a model for pressure dynamics and radial mass flow with basis in Darcy's law for flow through a porous medium [10]. The model was able to reproduce the internal pressure development measured by others [2], but the descriptions of the mechanical properties of the cable sheaths are somewhat over-simplified.

The present article starts by explaining how the geometry and physical properties of the various parts of a MIND cable and its surroundings can be modelled more accurately. These descriptions are implemented in a commercial software package (COMSOL Multiphysics). By selecting appropriate values for the material parameters and the geometry of a state-of-the-art MIND cable, the numerical model is used to simulate the internal pressures dynamics under different current loading, external pressures, and ambient temperatures. The model is verified against previously published pressure measurements obtained on 5-m long samples of this cable. Finally, the model is used to simulate cavity formation and the electric field distribution in two realistic operational cases that include ramping the current down, reversing the polarity and then ramping up again.

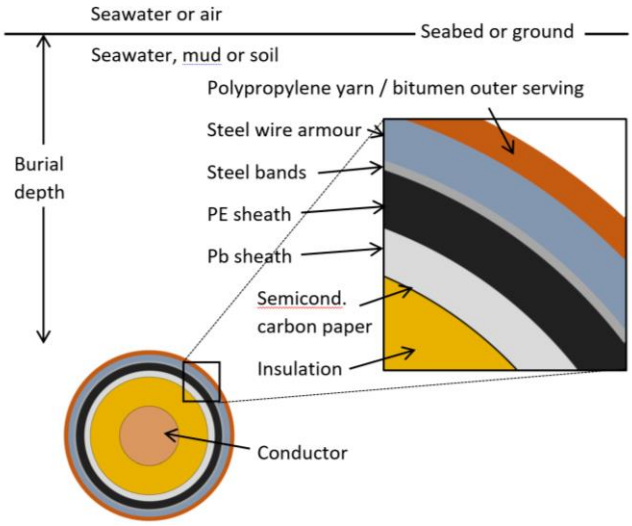

Figure 1. Geometry used for modelling internal pressures, temperatures and electric fields in the MIND cable insulation. The cable surface constitutes the interface between the 1-D and 2-D parts of the model.

2 MODEL

2.1 GEOMETRY

A geometry consisting of a 1-D axial symmetric model of the cable located inside a 12-m wide and 6-m deep 2-D area simulating the surroundings is created, see Figure 1. By changing the boundary conditions and the material properties of the 2-D part, all relevant environments can be considered, including a cable directly exposed to seawater or to air, or buried in mud at the seabed or in soil on land.

The cable model is built up as layers of homogeneous and isotropic materials. This implies that the stranded conductor is modelled as being solid, that the layered structure and the butt gaps of the mass-impregnated paper insulation are ignored, and that the steel bands are modelled as a thin-walled steel layer with a constant thickness. The semiconducting carbon paper on both sides of the insulation is modelled with the same properties as the insulation, except that it is considered electrically conducting, i.e., being at the same electrical potential as the conductor and the lead sheath, respectively. A few thin layers of bedding and serving between some of the layers shown in Figure 1, are simply ignored.

2.2 ELECTRIC AND THERMAL PROPERTIES

Most of the parameter values describing the electrical, thermal and mechanical properties of copper, lead, polyethylene and steel are included in the modelling software material library or easily obtained from the literature. The temperature dependency of the resistivity ρ of metals is expressed as

$$\rho = \rho_0[1 + \alpha_r(T - T_0)], \tag{1}$$

where ρ_0 is the resistivity at the temperature T_0 and α_r the temperature coefficient.

The temperature and field dependency of the electric conductivity σ of the mass-impregnated paper is given by the usual equation [11]:

$$\sigma = \sigma_0 \exp(\alpha T + \gamma E), \tag{2}$$

where T is temperature and E the electric field, and α and γ the associated coefficients.

2.3 MASS VISCOSITY AND PAPER PERMEABILITY

Szabo et al. [4] showed that radial flow of mass through the porous paper insulation of a MIND cable can be described by Darcy's law:

$$q = -\frac{k}{\mu}\frac{dp}{dr}. \tag{3}$$

Here q is the volumetric flux, k the permeability of the paper, μ the dynamic viscosity of the mass, and dp/dr the pressure gradient.

This article has been accepted for publication in a future issue of this journal, but has not been fully edited. Content may change prior to final publication. Citation information: DOI 10.1109/TDEI.2022.3173497, IEEE Transactions on Dielectrics and Electrical Insulation

The mass viscosity in the temperature range of interest has been measured by Szabo et al. [10] and was fit to a Williams-Landel-Ferry (WLF) type equation [12]:

$$\mu = \mu_{WLF} \exp\left[\frac{-A_{WLF}\,(T - T_{WLF})}{B_{WLF} + (T - T_{WLF})}\right] \quad (4)$$

to determine the four WLF parameters.

The density of the mass is slightly pressure and temperature dependent. The linear relationship

$$\rho_m = \rho_{m0} + \left(\frac{\partial \rho_m}{\partial T}\right)_p (T - T_0) + \left(\frac{\partial \rho_m}{\partial p}\right)_T (p - p_0) \quad (5)$$

used by Szabo et al. is applied. Here ρ_{m0} is the density at a reference pressure p_0 and reference temperature T_0.

The permeability of the lapped paper insulation to a radial flow of mass depends on a variety of cable design and manufacturing parameters, such as the lapping tension and the butt gap width. Hence, the permeability is most reliably determined experimentally on a case-to-case basis. One approach is to inject mass under pressure into the conductor of the cable and measure how the pressure underneath the lead sheath increases with time. (The mass flow through the conductor in the axial direction is much faster than the radial flow through the insulation, so compressed mass can be injected meters away from where the pressure under the lead sheath is recorded, simplifying the experiment.)

Figure 2 shows the results of such an investigation. The black lines are measured pressure and the red lines fits for determining the value for the paper permeability in Darcy's law. Equation (4) is applied for describing the temperature dependency of the viscosity.

The pressure under the lead sheath is extremely sensitive to small variations in the ambient temperature. Together with some minor difficulties with the temperature control arrangement, this led to the somewhat unsteady pressures seen in Figure 2, both for measured (black lines) and modelled/fitted (red lines).

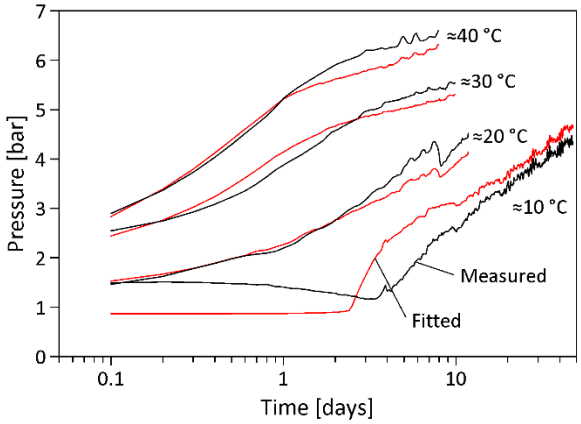

Figure 2. Pressure development (on a logarithmic time scale) under the lead sheath after injection of mass at around 6 bar into the conductor of a MIND cable at day zero. The experiment was repeated at four different temperature levels on an unloaded cable. Details about the setup, including the pressure sensors, cable temperature control and measurements etc. are given in a previous publication [7].

2.4 PAPER POROUSITY AND CAVITY FORMATION

The porosity is the volume fraction of the insulation that is available for the mass; for MIND cable insulation it is around 40%. The much larger thermal expansion coefficient of mass causes the internal pressure to rise rapidly when the insulation is warmed up, and the volume of the mass exceeds the available space in butt gaps and paper pores. Similarly, when cooling down the cable to low temperatures, thermal contraction causes a mass "deficit" that results in a falling pressure. In addition, the mass is slightly compressible, i.e., its density is not only changing with temperature but also with pressure, although to a much lesser degree.

At a certain intermediate temperature, here referred to as the "full-impregnation temperature", the volume of the mass is exactly sufficient to fill all butt gaps and pores in an unloaded cable under stationary conditions. The full-impregnation temperature is mainly determined by the cable design and manufacturing, but may not be precisely known.

In the modelling, the full-impregnation temperature is a parameter that must be assigned a value, and under certain conditions this value has a significant effect on the internal pressure dynamics.

The formation of shrinkage cavities that occurs at very low pressures is essentially an abrupt and local phase transition of small amounts of mass, from liquid to gaseous phase. This phenomenon is included in the model by making the porosity of the paper pressure dependent. Below the pressure levels where cavities are expected to form, the porosity is set to decrease linearly with decreasing pressure, see the schematic of Figure 3.

This can be thought of as a small fraction of the volume that mass occupies now is being "filled" with cavities. Or, in other words, the space available for the contracting mass is reduced, thereby reducing the resulting pressure drop. If no such measures were taken to account for the formation of cavities, the model would predict large negative pressures as the mass thermally contracts further from an already low pressure. This would result in an excessively large (and un-physical) pressure gradient across the insulation and a too high driving force for the radial mass flow.

When large pressure gradients exist across the insulation, the elasticity of the paper combined with a limited paper permeability will cause thin films of mass to temporarily accumulate between the paper layers. This increases the overall porosity. To account for this, the porosity is set to increase

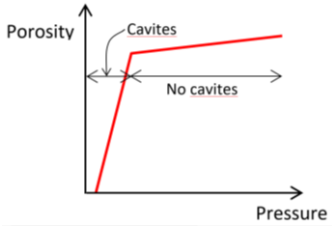

Figure 3. Pressure vs. porosity relationship applied in the model to account for the formation of cavities at low pressures (left part) and for accumulation of mass between the paper layers when there are large pressure gradients in the insulation (right part).

This article has been accepted for publication in a future issue of this journal, but has not been fully edited. Content may change prior to final publication. Citation information: DOI 10.1109/TDEI.2022.3173497, IEEE Transactions on Dielectrics and Electrical Insulation

slightly with increasing pressures above the levels where cavities may form, as shown in the right part of the plot in Figure 3. This reduces the pressure peaks at the innermost parts of the insulation after a load turn-on.

In conclusion, the modelling of the behavior of the mass-impregnated paper is in part based on Darcy's law and in part on empirical relations and parameter fitting using data obtained experimentally.

2.5 BOUNDARY CONDITIONS

Because the conductor is modelled as an incompressible and impermeable solid, no mass flows into or out of the conductor. When calculating mass flow and pressure distributions this simplification is justified by recognizing that stranded and compacted cable conductors typically have a fill factor of around 98%. This means that nearly all mass in the cable is in the insulation (which has a porosity of around 40%).

The lead sheath constitutes the outer, non-permeable boundary for the insulation. As opposed to the inner boundary, the cable casing (i.e., the lead and PE sheaths, and the steel bands) will deform if there is a high internal pressure, slightly enlarging the volume enclosing the insulation.

To calculate the pressure under the lead sheath, the model needs to keep track of the radial distribution of the mass in the insulation at any time. If the cable temperature is above the full-impregnation temperature, excess mass will end up as a film between the outermost paper layer and the lead sheath. This film exerts pressure on the cable casing; a higher temperature means a thicker film and a greater outward pressure. This outward mechanical force produced by thermal expansion of mass is balanced by the inward force generated by the casing. Obviously, the mechanical properties of the casing are crucially important for determining the radial deformation of the lead sheath and the pressure underneath.

2.6 MECHANICAL PROPERTIES OF CABLE CASING

Recent measurements of strains in the lead sheath and the steel bands of a cable casing under varying internal pressure revealed a complicated mechanical behavior [8]. The casing has viscoelastic properties, in essence implying that pressure changes result in immediate elastic deformations superimposed on plastic deformations that go on for weeks and months. Hence, accurately modelling the mechanical properties of the casing, including the interactions between the three layers of very different materials, is extremely challenging. In this work, a simple and semi-empirical approach is taken.

Figure 4 shows the crude model that is applied for describing the mechanical interaction between the cable casing and the insulation it encloses. The elastic properties of the steel bands and the lead sheath are represented as springs E_{Fe} and E_{Pb} with spring constants based on the E-modulus of steel and lead. (The PE sheath is much weaker, and its elastic properties are ignored.) The viscoelasticity of the lead sheath is modelled by a spring/damper series and parallel branch defined by C_{Plas}, E_{Visc} and C_{Visc}. The contact force between the lead and PE sheaths and the steel bands is modelled as a non-linear spring E_{Cont}.

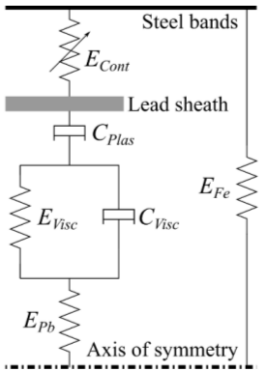

Figure 4. Four-parameter model for the mechanical behavior of the lead sheath, linked with the contact force model for interaction between lead and steel bands and the elasticity of the steel bands.

The values for the parameters E_{Visc}, C_{Visc}, C_{Plas} and E_{Cont} are preferably determined empirically from strain measurements obtained on a complete cable casing subjected to different internal pressures. Figure 5 shows the results of a laboratory experiment where the pressure under the lead sheath once every week was changed in 5-bar steps, in the range 1–25 bar. The strains at the inner surface of the lead sheath and at the outer surface of the steel bands were recorded, and the measured values were fitted to the model of Figure 4.

The measurements show several remarkable features. First, the lead sheath strain is up to 6–8 times larger than the steel band strain, indicating that the layers between the two strain gauges become compressed. Second, the lead strain changes more when stepping up and down at low pressures than at high pressures, demonstrating that non-linear effects are present. Third, the lead strain is not even close to stabilizing after a week at constant pressure, indicating that processes with time constants of the order of at least several weeks are at work.

Obviously, the crude mechanical model of Figure 4 is not able to replicate such a complex behavior fully and accurately. When fitting the parameters, obtaining reasonably correct time constants for the viscoelastic strain was prioritized, to a certain degree at the expense of reproducing the strain levels accurately.

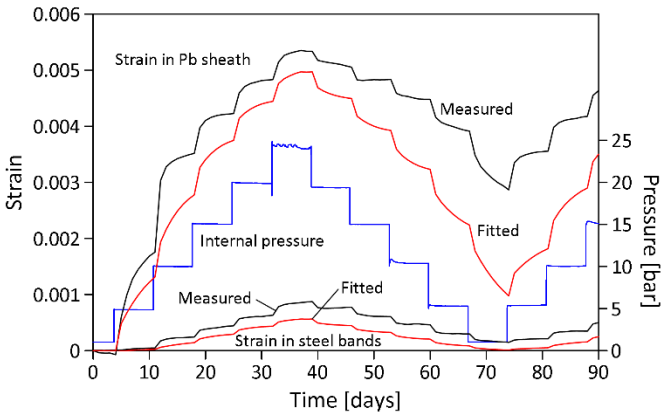

Figure 5. Measurements of tangential strain (black lines) at the inside of the lead sheath and at the outside of the steel bands of a MIND cable casing subjected to different internal pressures over a three-month period [8]. The red lines are best fits of E_{Visc}, C_{Visc}, C_{Plas} and E_{Cont} in the model shown in Figure 4.

This article has been accepted for publication in a future issue of this journal, but has not been fully edited. Content may change prior to final publication. Citation information: DOI 10.1109/TDEI.2022.3173497, IEEE Transactions on Dielectrics and Electrical Insulation

When modelling the internal pressure dynamics, the radial displacement of the lead sheath caused by the layer of "excessive" mass just underneath it, serves as input. The pressure under the lead sheath / in the outermost layers of the insulation is then determined from the response of the mechanical model.

The mechanical properties of the cable's armor and outer serving are disregarded, as these parts are not assumed to influence on the internal pressure of a cable in operation. Their thermal properties are however included when determining temperatures.

3 IMPLEMENTATION

COMSOL Multiphysics 5.5 [13] is used to create and solve a finite element model of the MIND cable and its surroundings. Temperatures are calculated using the "Heat Transfer" module in COMSOL and the appropriate initial and boundary conditions. When the cable is loaded the main heat source is the resistive losses in the conductor. The "Non-linear mechanics" module is used for modelling the mechanical behavior of the PE and lead sheaths. The radial mass flow and the associated pressure distribution in the insulation are calculated using the COMSOL module "Darcy's Law", and the electric field by means of the "Electric Currents" module. Electric potential is applied to the conductor, whereas the lead sheath is grounded.

4 VERIFICATION BY COMPARING WITH EXPERIMENTAL RESULTS

In recent efforts 5-m long samples of a modern 500 kV / 1400 A MIND HVDC subsea cable were subjected to a variety of ambient and loading conditions in the laboratory while the pressures at the innermost and outermost layers of the insulation were recorded [7–9]. The geometry and material properties of this cable are implemented in the numerical model described above, and the previously obtained measurements will be compared with simulation results to assess how well the model is able to replicate and predict the internal pressure behavior.

It should be emphasized that these cases are not emulating loading or ambient conditions/patterns typical for MIND cables in service; they are designed for exploring their internal pressure dynamics.

4.1 PARAMETER VALUES

Table 1 shows the dimensions of the cable, and Table 2 lists the material parameter values. The parameter values and relationships obtained empirically as a part of the present work are shown in Table 3 and in (6).

E_{Fe} and E_{Pb} in Figure 3 are determined from the cable dimensions given in Table 1 and Young's moduli. The E-modulus associated with the contact force acting between the lead and PE sheaths and the steel band is modelled as a second order polynomial (i.e., a non-linear spring):

$$E_{Cont}(t) = a + bt + ct^2 \quad (6)$$

where t is thickness of the mass film at the outside of the outermost paper layer of the insulation, equal to the radial displacement of the inner surface of the lead sheath. The coefficients are determined to $a = 3{\cdot}10^{-6}$ N/m, $b = 2{\cdot}10^{12}$ N/m^2, and $c = 5{\cdot}10^{16}$ N/m^3.

The pressure vs porosity relationship (see Figure 3) is defined by assuming that cavities form below 0.02 bar (the kink in Figure 3). At this pressure, the porosity is 0.4 (i.e., 40%). At higher pressures, the porosity is set to increase linearly at a rate of 0.0001 per bar, while at lower pressure it decreases at a rate of 0.375 per bar.

The full-impregnation temperature is set to 10 ºC.

Table 1. Cable dimensions (see Figure 1).

Material/layer	Thickness [mm]	Radius [mm]
Copper conductor		23.15
Semiconducting carbon paper	0.4	23.55
Mass-impregnated paper insulation	20.15	43.7
Semiconducting carbon paper	0.9	44.6
Lead sheath	3.3	47.9
Polyethylene (PE) sheath	3.3	51.2
Steel bands	2 x 0.4	52
Steel wires armor	2 x 3	58
Polypropylene yarn / bitumen outer serving	5	63

Table 2. Material properties.

Material/property	Symbol	Value	Ref.
Resistivity of Cu @ 293.15 K	ρ_0	$1.724{\cdot}10^{-8}$ Ωm	[14]
; temperature dependency	α_r	$3.93{\cdot}10^{-3}$ K^{-1}	[14]
Thermal cond. of Cu		401 W/(m K)	[15]
Heat capacity of Cu		385 J/(kg K)	[15]
Density of Cu		8960 kg/m^3	[15]
Electrical cond. of insulation	σ_0	$0.57{\cdot}10^{-16}$ S/m	[16]
; temperature dependency	α	0.11 K^{-1}	[16]
; field dependency	γ	0.035 mm/kV	[16]
Viscosity of mass; see Eq. (4)	μ_{WLF}	2.1 Pa s	[10]
; see Eq. (4)	A_{WLF}	8.15	[10]
; see Eq. (4)	B_{WLF}	125 K	[10]
; see Eq. (4)	T_{WLF}	323 K	[10]
Density of mass @ 273 K / 1 bar	ρ_{m0}	939 kg/m^3	[10]
; pressure depend. @ 273 K / 1 bar	$d\rho_m/dp$	$4.7{\cdot}10^{-7}$ s^2/m^2	[10]
; temp. depend. @ 273 K / 1 bar	$d\rho_m/dT$	-0.6 kg/(K m^3)	[10]
Thermal cond. of insulation		0.211 W/(m K)	[16]
Heat capacity of insulation		2110 J/(kg K)	[16]
Density of insulation (porosity: 0.4)		946 kg/m^3	[16]
Thermal cond. of Pb		35.3 W/(m K)	[13]
Heat capacity of Pb		128 J/(kg K)	[13]
Density of Pb		11300 kg/m^3	[13]
Young's modulus of Pb		16 GPa	[13]
Thermal cond. of PE		0.4 W/(m K)	[17]
Heat capacity of PE		2264 J/(kg K)	[18]
Density of PE		1060 kg/m^3	[16]
Thermal cond. of steel bands		44.5 W/(m K)	[13]
Heat capacity of steel bands		484 J/(kg K)	[18]
Density of steel bands		7850 kg/m^3	[13]
Young's modulus of steel bands		205 GPa	[13]
Thermal cond. of yarn/bitumen		0.17 W/(m K)	[16]
Heat capacity of yarn/bitumen		1980 J/(kg K)	[16]
Density of yarn/bitumen		1010 kg/m^3	[16]

Table 3. Paper permeability and mechanical properties of the sheaths.

Material/property	Symbol	Value
Permeability of paper; ref. Figure 2	k	$1.41{\cdot}10^{-16}$ m^{-2}
Mechanical prop. of sheaths; see Figure 4	E_{Visc}	10^9 N/m
; see Figure 4	C_{Visc}	10^{15} Ns/m
; see Figure 4	C_{Plas}	10^{17} Ns/m

This article has been accepted for publication in a future issue of this journal, but has not been fully edited. Content may change prior to final publication. Citation information: DOI 10.1109/TDEI.2022.3173497, IEEE Transactions on Dielectrics and Electrical Insulation

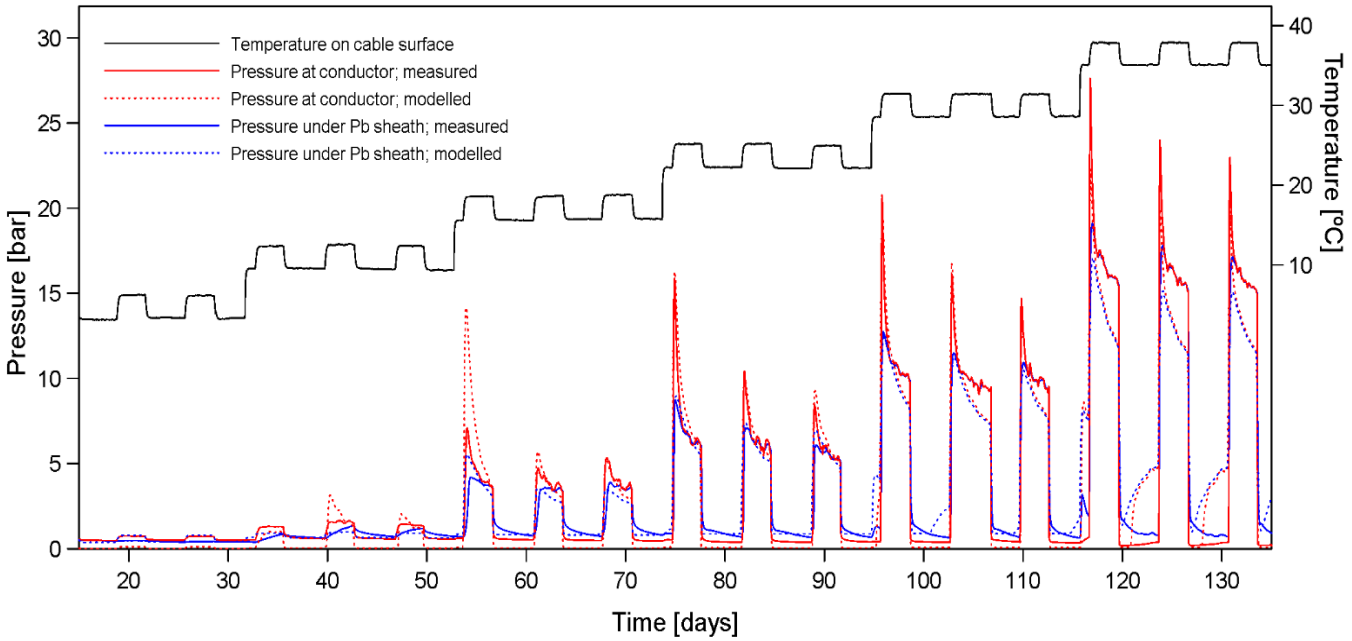

Figure 6. Comparison between simulations (dashed lines) and measurements (solid lines) of the internal pressure in the innermost (red) and outermost (blue) layers of the insulation during three days on / four days off cycling with rated load current. The ambient temperature was increased in steps of 7 ºC every three weeks. Details about the experimental setup and procedures have been described earlier [7].

4.2 LOAD CYCLING AT DIFFERENT AMBIENT TEMPERATURES

Figure 6 shows measured and modelled pressure at the innermost and outermost parts of the insulation during load cycling. The current on and off periods are clearly seen as rises and drops in the recorded pressure and in the temperature profile. The temperature on the cable surface was controlled by circulating a liquid in pipes wound around the cable sample, but this arrangement was not able to maintain a perfectly constant cable surface temperature; it rose some 3 ºC during the loading parts of the cycles. This recorded cable surface temperature was used as a boundary condition in the simulation. The ambient pressure was 1 bar (i.e., atmospheric).

Considering the complexity of the phenomena involved, the overall agreement between the modelled and measured pressures is good. Most features observed experimentally are recreated by the model, including: i) The large and rapid pressure rises/drops after load turn-ons/offs (due to thermal expansion and contraction of the mass); ii) The pressure difference across the insulation disappearing sooner at high temperatures than at low (explainable as a faster radial mass migration when the mass is warm and its viscosity low); iii) The higher peak pressure in the first load cycle at a new temperature level compared to that of the two cycles that follow (indicating that some of the mass from the innermost insulation layers has not yet returned); iv) The pressure becomes very low during the unloaded part of the cycles also at high ambient temperatures (presumably because the lead and PE sheaths have been slowly deformed in the preceding weeks, yielding a larger volume available for the insulation).

The latter phenomenon is particularly interesting when assessing the risk of creating potentially harmful shrinkage cavities in the insulation, as it suggests that cavities may form also at high ambient temperature (as here at 35–38 ºC).

4.3 LOAD CYCLING AT DIFFERENT AMBIENT PRESSURES

To clarify the effects of an external water pressure on the internal pressure of a subsea MIND cable, measurements were carried out on a cable installed in a pressure vessel [9]. Figure 7 shows measured and modelled pressures at both sides of the insulation during load cycling in atmospheric pressures and under external pressures corresponding to 30, 60 and 90 m water depth. Again, the temperature measured on the cable surface was used as a boundary condition in the modelling.

The discrepancy between measured and modelled pressures is considerably greater here than in the case presented in Figure 6. At elevated ambient pressures, the internal pressure excursions predicted by the model exceed those measured. The pressure in the innermost parts of the insulation—both in the model and in the measurements—immediately after the load turn-offs drops to levels far below the ambient pressure. However, in the measurements at 4, 7 and 10 bar ambient it does not become lower than 2–5 bar, indicating that cavities are not created. The modelling, in contrast, shows pressure drops to virtually zero in these cases, suggesting that cavities may form.

In general, the model is clearly too simple to accurately predict the pressure dynamics as this involves complex phenomena such as liquid-to-gas phase transition, viscous flow in a porous medium, non-linear stress-strain behavior of solids, etc. A slightly inaccurate modelling of the compressibility and elasticity of the paper may have a greater effect at elevated

This article has been accepted for publication in a future issue of this journal, but has not been fully edited. Content may change prior to final publication. Citation information: DOI 10.1109/TDEI.2022.3173497, IEEE Transactions on Dielectrics and Electrical Insulation

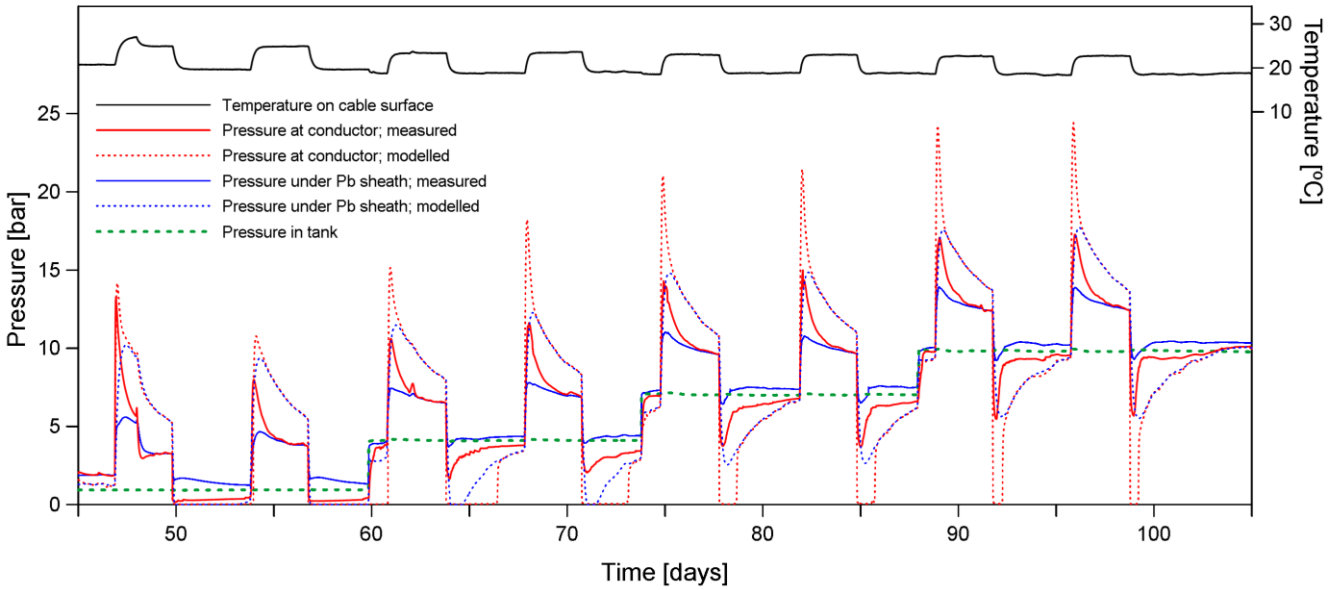

Figure 7. Comparison between simulations (dashed lines) and measurements (solid lines) of the internal pressure in the innermost (red) and outermost (blue) layers of the insulation during three days on / four days off cycling with rated load current. The ambient pressure (green dashed line) was increased in steps of 3 bar every second week to simulate different water depths. The cable surface temperature was kept at around 20 ºC, becoming somewhat higher in the loading part or the cycles. Details about the experimental setup and procedures have been presented in an earlier publication [9].

external pressures than at 1 bar, and this may, at least in part, explain the larger discrepancies between measured and modelled pressures at elevated external pressures.

Still, the modelling is considered useful in understanding the insulation system as the main characteristics of the pressure dynamics are reasonably well reproduced, e.g., the overall shape of the pressure profiles, the ratio between the pressure at the innermost and outermost parts of the insulation, and that the pressure changes due to the load cycling become superimposed on the external water pressure.

Of particular interest is that both measurements and modelling suggest that the internal pressure becomes the same throughout the insulation and always asymptotically approaches the external pressure, both when the cable is loaded and unloaded (although the three days loading period is somewhat short to fully confirm this).

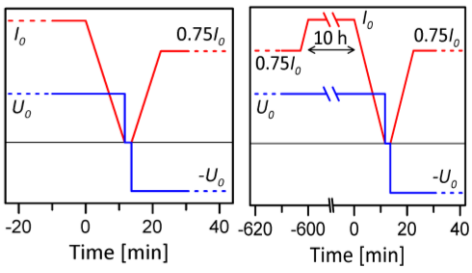

Figure 8. Current (red) and voltage (blue) applied in the two cases modelled. In Case I (left) the cable has been operating with rated current and voltage for infinitively long before the current is ramped down. Case II (right) has also reached steady state but with 75% load, before the load is temporarily raised to 100% for 10 hrs, before the down-ramping starts. From then on, the two cases are similar: current is ramped down to zero, polarity is reversed after a 2-min "resting time", and current is ramped up to 75% of rated current. Time $t = 0$ is set as the start of the load reduction.

5 SIMULATION OF SERVICE-LIKE CASES

The loading of many HVDC links changes rapidly, both regarding the amount of power transmitted and the direction of the power flow. Figure 8 shows two realistic patterns and how this can be achieved. The current is here ramped down from full load to zero at a rate of 60 MW/min, voltage is then turned off and the cable grounded for two minutes, before applying the rated voltage of the opposite polarity and ramping up the load at 60 MW/min. Hence, these cases include both a large and rapid load reduction and a polarity reversal. The former comes with a risk of forming shrinkage cavities, the latter causes a temporary but substantial increase in the electric field in the innermost parts of the insulation due to space charges [5]. Hence, there is here a compounding effect of the risk by cavity formation and high dielectric stresses in the innermost parts of the cable insulation.

The temperature, electric field and pressure in the insulation are calculated for these two cases by applying the model. The environmental conditions correspond to an un-trenched cable directly exposed to shallow sea water, i.e., ambient pressure is 1 bar, and the cable surface temperature is kept constant at 10 ºC.

The graphs in Figure 9 show some of the simulation results. The plotted "void fraction" is calculated as the "mass deficit" in the innermost 0.4 mm of the insulation divided by the combined butt gap volume in the same area. The butt gap width is assumed to be 10% of the paper tape width, and the volume of the mass to be 40% of the insulation volume.

Several interesting observations and interpretations can be made from these graphs:

This article has been accepted for publication in a future issue of this journal, but has not been fully edited. Content may change prior to final publication. Citation information: DOI 10.1109/TDEI.2022.3173497, IEEE Transactions on Dielectrics and Electrical Insulation

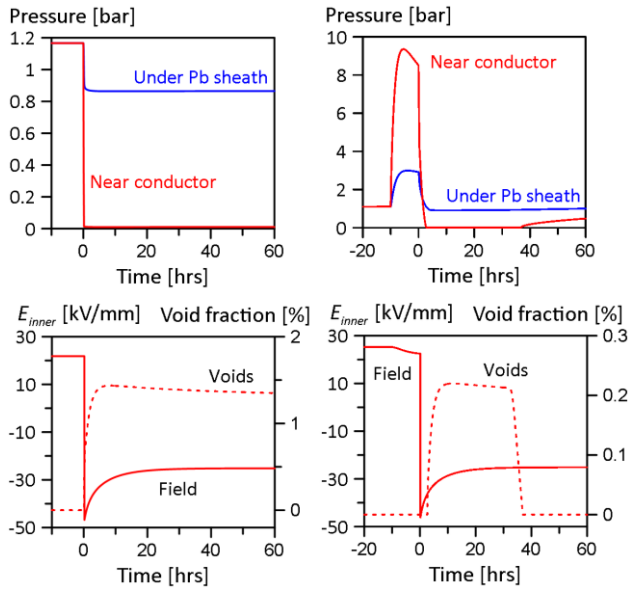

Figure 9. Case I (left graphs) and Case II (right graphs) simulation results. The pressure development in the innermost and outermost parts of the insulation before the load change and in the 60 hrs afterwards are seen in the upper graphs. The lower graphs show the electrical field in the innermost insulation layers as well as the combined shrinkage void volume divided by the butt gap volume of the innermost five paper layers (or 0.4 mm of insulation). Note that the time axes extend orders of magnitude longer than those of Figure 8.

- The loading of the two cases was identical in the last 10 hrs before the ramp-down initiated at $t = 0$. Still, the pressure at $t = 0$ and the void fraction later generated in the innermost layers deviate considerably between the two cases, indicating that the loading history days back influences greatly on these phenomena.
- Even though the pressure drop that starts at $t = 0$ is far less in Case I than in Case II, significantly more voids are formed (approximately 1.5% vs. 0.2% of the butt gap volume). The reason is that the lead and PE sheaths during the long time at I_0 have suffered greater *viscoelastic* deformations than at $0.75 \cdot I_0$, giving more space for the insulation in Case I. The 10 hrs at I_0 leading up to $t = 0$ in Case II result mainly in additional *elastic* deformations that disappear when current is ramped down and the mass contracts thermally.
- When the new load of $0.75I_0$ is established, the pressure difference existing between the innermost and outermost insulation layers sets up an inwardly directed migration (a "back flow") of mass that eventually will fill the cavities. However, the modest pressure difference (about 1 bar in both cases) causes the flow rate to be low. In Case II it takes around 34 hrs before the voids near the conductor disappear and the pressure starts increasing, see the upper and lower right-hand graphs of Figure 9. In Case I, which had more voids in the innermost part of the insulation, this stage is not reached within the time covered by the simulation.
- In Case I the formation of cavities coincides in time with when the field strength reaches its maximum, i.e., immediately after the polarity reversal. In Case II, the first voids appear a few hours later when the space charge redistribution is well under way and the field has become considerably lower. Hence, from this perspective Case II should be less stressful for the cable than Case I.

A final and important comment is that internal pressure drops to virtually zero combined with the high dielectric stress associated with a polarity reversal are not necessarily and in all cases associated with aging of the insulation. If the "mass deficit" is distributed as many and minute voids and/or the time with low internal pressure is short, the energy of any partial discharges may be too low to damage the insulation. It may be speculated that a combination of a large "mass deficit", an extended time at a low pressure, and poorly compacted paper layers may be more dangerous as this may allow small cavities to move around and combine to larger ones that result in more powerful and hazardous partial discharges.

6 CONCLUSIONS

The developed finite element model for temperature, electric field and pressure dynamics replicates the pressure behavior of the insulation of full-scale HVDC subsea cables subjected to a variety of loading and environmental conditions reasonably well. The model can be applied to identify when potentially harmful shrinkage cavities form in the insulation, but the complexity of the processes involved (liquid-to-gas phase transition of the mass, viscous flow of mass in and between lapped porous paper, the non-linear stress-strain behavior of the lead sheath, etc.) causes the predictions to be qualitative rather than quantitative.

ACKNOWLEDGMENT

This work was supported in part by the Norwegian Research Council, Statnett, Nexans Norway, Fingrid, and Svenska Kraftnät under contract no. 256405/E20.

REFERENCES

[1] T. Worzyk, Submarine Power Cables: Design, Installation, Repair, Environmental Aspects, Berlin, Heidelberg, Germany: Springer, 2009.

[2] A. Eriksson *et al*, "Development work concerning testing procedures of mass-impregnated HVDC cables," *Int. Council Large Electric Systems (CIGRÉ)*, 1994, Paper no. 21-206

[3] G. Evenset, J. Sletbak, and O. Lillevik, "Cavity formation in mass-impregnated high voltage direct current cable insulation," *IEEE Conf. Electr. Phenom. (CEIDP)*, 1998, pp. 554–559

[4] G. Evenset and G. Balog, "The breakdown mechanism of HVDC mass-impregnated cables," *Int. Council Large Electric Systems (CIGRÉ)*, 2000, Paper no. 21-303.

[5] M. Runde *et al*, "Cavity formation in mass-impregnated HVDC subsea cables—Mechanisms and critical parameters," IEEE Electr. Insul. Mag., vol. 30, pp. 22–33, 2014.

[6] CIGRÉ Working Group 21-02, "Recommendations for tests of power transmission DC cables for a rated voltage up to 800 kV," Electra, no. 189, pp. 39–55, 2000.

[7] M. Runde *et al*, "Internal pressures and pressure gradients in mass-impregnated HVDC cables during current cycling," IEEE Trans. Dielectr. Electr. Insul., vol. 27, pp. 915–923, 2020.

[8] M. Runde *et al*, "Plastic deformations of the sheaths of mass-impregnated HVDC cables and their effect on the internal pressure," CIGRÉ Sc. Eng., vol. 21, pp. 14–25, 2021.

[9] M. Runde *et al*, "Internal pressure dynamics of mass-impregnated HVDC subsea cables at different sea depths," CIGRÉ Sc. Eng., vol. 24, pp. 1–11, 2022.

[10] P. Szabo, O. Hassager, and E. Strøbech, "Modelling of pressure effects in HVDC cables," IEEE Trans. Dielectr. Electr. Insul., vol. 6. pp. 845–851, 1999.
[11] CIGRÉ Task Force B1.16, "Addendum to Recommendations for tests of power transmission DC cables for a rated voltage up to 800 kV," Electra, no. 218, pp. 39–45, 2005.
[12] R. B. Bird, R. C. Armstrong, and O Hassager, Dynamics of Polymer Liquids, Vol. 1: Fluid Mechanics, New York: John Wiley & Sons, 1987.
[13] COMSOL Multiphysics, Available: http://www.comsol.com
[14] Electric cables – Calculation of the current rating – Part 1-1: Current rating equations (100% load factor) and calculation of losses – General, Int. Standard IEC 60287-1-1, 2014.
[15] W. M. Haynes, CRC Handbook of chemistry and physics, Boca Raton: CRC Press, 2014
[16] L. Lervik, Nexans Norway, private communication, 2017.
[17] Calculation of thermally permissible short-circuit currents, taking into account non-adiabatic heating effects, Int. Standard IEC 60949, 1988.
[18] Calculation of the cyclic and emergency current rating of cables. Part 2: Cyclic rating of cables greater than 18/30 (36) kV and emergency ratings for cables of all voltages, Int. Standard IEC 60853-2, 1989.